

Natural inflation in Palatini $F(R)$

N. Bostan,^a R. H. Dejarah,^b C. Dioguardi,^{c,d} and A. Racioppi^d

^aDepartment of Physics, Faculty of Science, Marmara University, 34722 Istanbul, Türkiye

^bDepartment of Physics, Faculty of Science, Ankara University, 06100 Ankara, Türkiye

^cTallinn University of Technology, Akadeemia tee 23, 12618 Tallinn, Estonia

^dNational Institute of Chemical Physics and Biophysics, Rävåla 10, 10143 Tallinn, Estonia

E-mail: nilay.bostan@marmara.edu.tr, rafid.dejarah@gmail.com,
christian.dioguardi@kbf.ee, antonio.racioppi@kbf.ee

Abstract. $F(R)$ Palatini gravity provides a robust framework for constructing viable inflationary potentials. In this study, we examine natural inflation and show that its consistency with observational data can be restored when the model is embedded within $F(R)$ Palatini gravity, specifically for $F(R) = R + \alpha R^n$ with $7/4 \lesssim n \leq 2$. For completeness, we also demonstrate that models with $n > 2$ do not yield comparable improvements, achieving partial agreement with the data only in the limit $n \rightarrow 2$.

Keywords: natural inflation, Palatini gravity

Contents

1	Introduction	1
2	Palatini $F(R)$ theories	2
3	Natural inflation for $n \leq 2$	4
4	Natural inflation for $n > 2$	8
5	Conclusions	10

1 Introduction

The Standard Model of Cosmology is built on the cosmological principle, which asserts that the Universe is homogeneous and isotropic on sufficiently large scales. Observations of the Cosmic Microwave Background (CMB) [1], large galaxy surveys [2, 3], and the distribution of large-scale structures strongly support this principle, showing that the Universe is remarkably uniform across hundreds of megaparsecs. Nevertheless, explaining this uniformity, along with the near-flat geometry of the Universe and the absence of exotic relics, requires a mechanism operating in the very early Universe. The most compelling solution is a brief phase of rapid accelerated expansion [4–7], commonly referred to as *inflation*. In addition to resolving these issues, inflation provides a natural origin for the tiny primordial fluctuations that later evolve into galaxies, clusters, and the cosmic web.

A simple realization of inflation is through a scalar field, called the *inflaton*, whose potential energy drives the accelerated expansion. The detailed shape of the inflaton potential determines both the duration of inflation and the properties of the resulting primordial perturbations. High-precision measurements of the CMB by *Planck* and *BICEP/Keck* [8, 9] have ruled out the simplest minimally coupled models, motivating the exploration of more elaborate constructions. Among these, *natural inflation* [10] stands out as a particularly elegant scenario: the inflaton is realized as a pseudo-Nambu-Goldstone boson with a periodic potential. This structure naturally keeps the potential flat, reducing the need for fine-tuning. Although theoretically appealing, the original natural inflation model is now in tension with observations, prompting numerous extensions and modifications to reconcile it with current data [11–27].

A promising approach is to embed inflation in the Palatini formulation of gravity (e.g. [28–31] and refs. therein), in which the metric and connection are treated as independent variables. This framework modifies the way the scalar field interacts with gravity, potentially altering the predictions for inflation, often reducing the required field excursion and relaxing observational constraints from the CMB. Within this context, $F(R)$ theories provide a versatile extension (e.g. [32–46] and refs. therein), allowing the effective inflationary potential in the Einstein frame to be adjusted. In this work, we focus on models in which the potential remains bounded and positive, as in natural inflation, demonstrating that such scenarios can reconcile theory with observational data while preserving the desirable theoretical properties of the original model.

2 Palatini $F(R)$ theories

Let us begin by considering the following action, minimally coupled to $F(R)$ gravity, where we set the reduced Planck mass $M_P \equiv 1$ and adopt a space-like metric signature:

$$S_J = \int d^4x \sqrt{-g_J} \left[\frac{1}{2} F(R(\Gamma)) - \frac{1}{2} g_J^{\mu\nu} \partial_\mu \phi \partial_\nu \phi - V(\phi) \right], \quad (2.1)$$

where ϕ is the inflaton scalar field. Here, $g_J^{\mu\nu}$ denotes the Jordan-frame metric, and $R(\Gamma) = g_J^{\mu\nu} R_{\mu\nu}(\Gamma)$ is the Ricci scalar obtained by contracting the metric-independent Ricci tensor with the Jordan-frame metric. This framework has been extensively studied in [38] for positive-definite potentials, and in [41] for well-defined negative potentials. A similar setup for more general functions of the form $F(R, X)$, with $X = -g_J^{\mu\nu} \partial_\mu \phi \partial_\nu \phi$, was considered in [42]. In this work, we focus on the complementary case in which the scalar potential is bounded from above, specifically considering natural inflation.

As shown in [38], the action (2.1) can be rewritten in the Einstein frame, where the gravitational action is linear in the Ricci scalar. As a first step, we introduce an auxiliary field ζ to rewrite the action as:

$$S_J = \int d^4x \sqrt{-g_J} \left[\frac{1}{2} (F(\zeta) + F'(\zeta)(R - \zeta)) - V(\phi) \right], \quad (2.2)$$

where the prime denotes differentiation with respect to the argument. Next, we perform the conformal transformation:

$$g_{E\mu\nu} = F'(\zeta) g_{J\mu\nu}, \quad (2.3)$$

where $g_{E\mu\nu}$ is the Einstein-frame metric. Since the Ricci tensor is independent of the metric in the Palatini formulation, this transformation leads to:

$$S_E = \int d^4x \sqrt{-g_E} \left[\frac{1}{2} R_E - \frac{1}{2} g_E^{\mu\nu} \partial_\mu \chi \partial_\nu \chi - U(\chi, \zeta) \right], \quad (2.4)$$

where we have defined a canonically normalized scalar field:

$$\frac{\partial \chi}{\partial \phi} = \sqrt{\frac{1}{F'(\zeta)}}, \quad (2.5)$$

and an effective scalar potential:

$$U(\chi, \zeta) = \frac{V(\phi(\chi))}{F'(\zeta)^2} - \frac{F(\zeta)}{2F'(\zeta)^2} + \frac{\zeta}{2F'(\zeta)}. \quad (2.6)$$

The equation of motion for the auxiliary field is obtained by varying (2.6) with respect to ζ , which yields:

$$2F(\zeta) - \zeta F'(\zeta) - \partial^\mu \phi \partial_\mu \phi F'(\zeta) - 4V(\phi) = 0. \quad (2.7)$$

In general, this equation cannot be solved explicitly for ζ . However, for the computation of inflationary observables, we can adopt the slow-roll approximation, in which the energy of the scalar field is dominated by its potential. Under this approximation, Eq. (2.7) reduces to:

$$G(\zeta) = V(\phi), \quad (2.8)$$

with

$$G(\zeta) \equiv \frac{1}{4} [2F(\zeta) - \zeta F'(\zeta)] . \quad (2.9)$$

Although it is generally not possible to find an explicit solution for $\zeta(\phi)$, one can use (2.8) in (2.6) to express the Einstein-frame potential as function of just ζ :

$$U(\zeta) = \frac{\zeta}{4F'(\zeta)} . \quad (2.10)$$

The slow-roll parameters can then be computed as derivatives of $U(\zeta)$ with respect to the canonical field χ :

$$\epsilon(\zeta) = \frac{1}{2} \left(\frac{\partial U / \partial \chi}{U} \right)^2 = \frac{1}{2} g^2 \left(\frac{U'}{U} \right)^2 , \quad (2.11)$$

$$\eta(\zeta) = \frac{\partial^2 U / \partial \chi^2}{U} = \frac{g g' U' + g^2 U''}{U} , \quad (2.12)$$

where

$$g(\zeta) \equiv \frac{\partial \zeta}{\partial \chi} = \sqrt{F'(\zeta)} \left(\frac{\partial G}{\partial \zeta} \frac{\partial V^{-1}}{\partial G} \right)^{-1} . \quad (2.13)$$

The CMB observables are then given by:

$$r(\zeta) = 16 \epsilon(\zeta) = 8 g^2 \left(\frac{U'}{U} \right)^2 , \quad (2.14)$$

$$n_s(\zeta) = 1 + 2 \eta(\zeta) - 6 \epsilon(\zeta) = 1 + \frac{2g}{U^2} (g' U' U + g U'' U - 24 g U'^2) , \quad (2.15)$$

$$A_s(\zeta) = \frac{U}{24 \pi^2 \epsilon(\zeta)} = \frac{U^3}{12 \pi^2 g^2 U'^2} . \quad (2.16)$$

Finally, the number of e-folds can be expressed as follows:

$$N_e = \int_{\chi_{\text{end}}}^{\chi_N} \frac{U}{\partial U / \partial \chi} d\chi = \int_{\zeta_{\text{end}}}^{\zeta_N} \frac{U}{g^2 \partial U / \partial \zeta} d\zeta , \quad (2.17)$$

where ζ_{end} is defined by $\epsilon(\zeta_{\text{end}}) = 1$, and ζ_N corresponds to the field value at which the pivot scale exits the horizon. Further details on this formalism can be found in [38].

In this work, we consider as the Jordan-frame potential, the natural inflation one:

$$V(\phi) = \Lambda^4 \left[1 + \cos \left(\frac{\phi}{M} \right) \right] , \quad (2.18)$$

together with a polynomial $F(R)$ function of the form:

$$F(R) = R + \alpha R^n . \quad (2.19)$$

Due to the distinct properties of $G(\zeta)$, we analyze the cases $n \leq 2$ and $n > 2$ in separate sections.

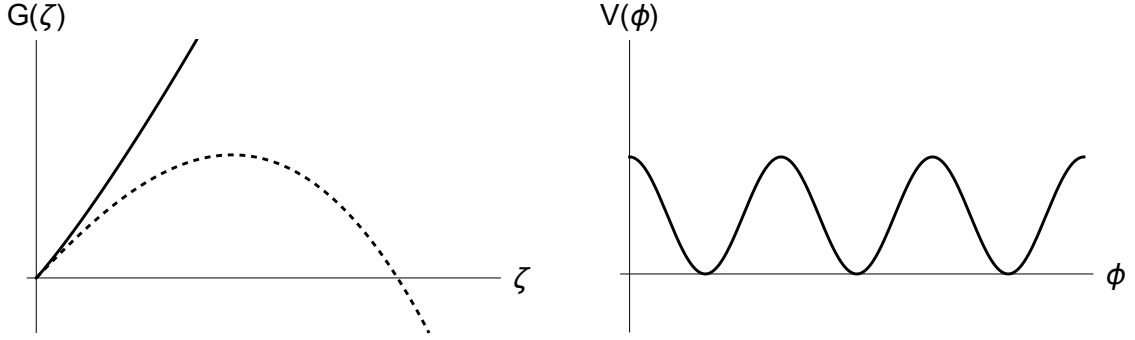


Figure 1: Reference plots of $G(\zeta)$ (left), generated using $F(R) = R + \alpha R^n$ for $n \leq 2$ (continuous) and $n > 2$ (dashed), and the natural inflation potential $V(\phi)$ (right). Note that, for $n > 2$ the condition $G(\zeta) = V(\phi)$ can be satisfied for any value of ϕ , provided that the local maximum of G exceeds the maximum of V .

3 Natural inflation for $n \leq 2$

For the class of $F(R)$ models defined in Eq. (2.19), we obtain from Eq. (2.9) that:

$$G(\zeta) = \frac{1}{4} (\zeta + \alpha(2-n)\zeta^n), \quad (3.1)$$

which is positive and monotonically increasing for $\zeta > 0$, provided that $1 < n \leq 2$. The case $n = 2$ was already studied explicitly in [15, 32]. Therefore, we focus on the range $1 < n < 2$. To obtain expressions for the CMB observables, we adopt the formalism derived in [38] and briefly outlined in Section 2. In terms of ζ_N , we then have:

$$n_s(\zeta_N) = 1 - \frac{16\Lambda^4 - \zeta_N}{M^2\zeta_N G'(\zeta_N)} - \frac{2\alpha(2-n) [4\Lambda^4(3-n) - \zeta_N(2-n)] \zeta_N^{n-2}}{M^2 G'(\zeta_N)} - \frac{\alpha^2(n-2)^2(2n-3)\zeta_N^{2n-2}}{M^2 G'(\zeta_N)}, \quad (3.2)$$

$$r(\zeta_N) = \frac{128G(\zeta_N)(2\Lambda^4 - G(\zeta_N))}{M^2\zeta_N^2 F'(\zeta_N)}, \quad (3.3)$$

$$A_s(\zeta_N) = \frac{M^2\zeta_N^3}{768\pi^2 G(\zeta_N)(2\Lambda^4 - G(\zeta_N))}, \quad (3.4)$$

$$N_e(\zeta_N) = \int_{\zeta_{\text{end}}}^{\zeta_N} \frac{M^2\zeta G'(\zeta)}{4G(\zeta)(2\Lambda^4 - G(\zeta))} d\zeta. \quad (3.5)$$

The numerical results for the $n \leq 2$ scenario are shown in Figs. 2 and 3, corresponding to $N_e = 50$ and $N_e = 60$, respectively. Panel (a) shows r vs. n_s , panel (b) shows r vs. $\log_{10}(\alpha)$, panel (c) shows n_s vs. $\log_{10}(\alpha)$, and panel (d) shows Λ vs. $\log_{10}(\alpha)$, for $n = 3/2$ (continuous), $n = 7/4$ (dashed), $n = 31/16$ (dot-dashed), and $n = 2$ (dotted), with $M = 5$ (orange), $M = 6$ (blue), $M = 10$ (green), and $M = 500$ (red). The black line denotes the original prediction of natural inflation, while the dots show the predictions for fixed M ; larger dots correspond to increasing values of M . The amplitude of the power spectrum, A_s , is fixed to its observed value $A_s \simeq 2.1 \cdot 10^{-9}$ [8]. Contours indicate the 68% and 95% confidence levels based on the

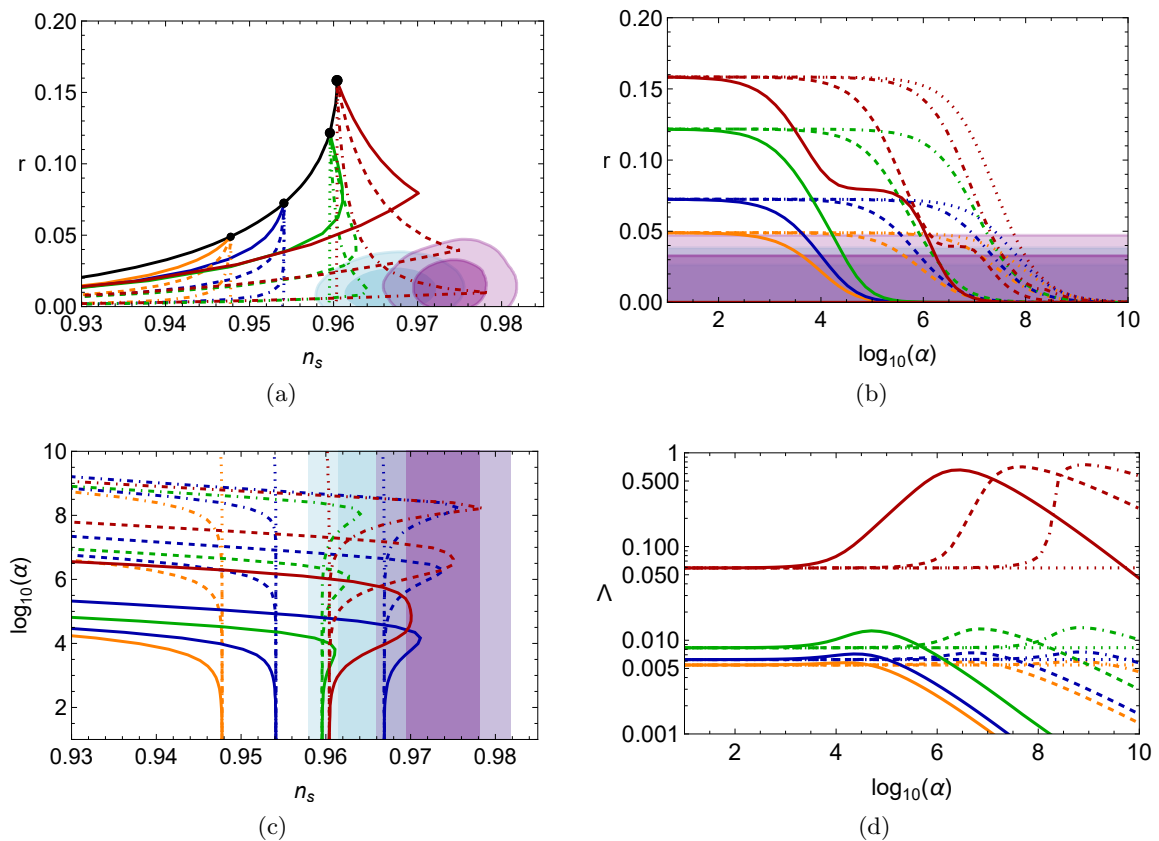


Figure 2: (a) r vs. n_s , (b) r vs. $\log_{10}(\alpha)$, (c) n_s vs. $\log_{10}(\alpha)$, and (d) Λ vs. $\log_{10}(\alpha)$ for $n \leq 2$ and $N_e = 50$ with $n = 3/2$ (continuous), $n = 7/4$ (dashed), $n = 31/16$ (dot-dashed), and $n = 2$ (dotted), and with $M = 5$ (orange), $M = 6$ (blue), $M = 10$ (green), and $M = 500$ (red). The black line indicates the original prediction for natural inflation, while the dots correspond to predictions for fixed M , with larger dots representing increasing M . Contours display the 68% and 95% confidence levels based on the latest combinations from BICEP/Keck [9] (cyan), and ACT collaborations [47] (purple).

latest combinations from BICEP/Keck [9] (cyan), and ACT collaborations [47] (purple). All plots were obtained by fixing (M, n) and varying α in the range $0 < \alpha < 10^{10}$. As it is well known, the shift in N_e does not alter the dependence on the free parameters of the model¹, and therefore the following discussion applies to both Figs. 2 and 3.

In panel (a), we observe that as n approaches 2, the predictions move towards lower values of r , while n_s spans a larger range. Panel (b) shows that the tensor-to-scalar ratio r decreases for increasing α , similar to the behavior observed for positive unbounded potentials in [38]. In panel (c), for $M \gtrsim 10$, n_s increases until reaching a maximum value that depends on both M and n , and then decreases towards values disfavored by both combinations. This is reflected in panel (b) by a temporary plateau in r , most noticeable for $M = 500$ and $n = 3/2, 7/4$. Such behavior corresponds to the “knee” shape of the r vs. n_s predictions in panel

¹Larger values of N_e probe field values farther from the end of inflation, where the potential is flatter, naturally leading to smaller ϵ and, consequently, lower r and higher n_s , while leaving the dependence on M , α , and n unchanged.

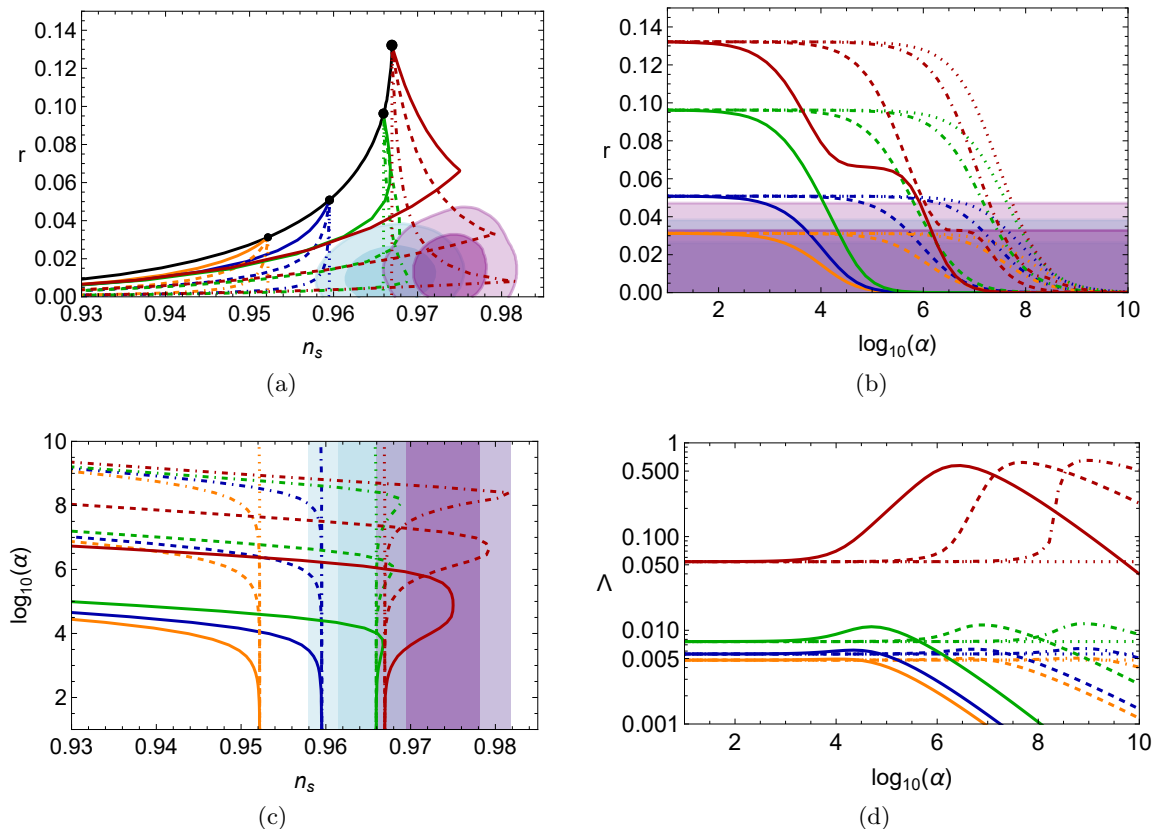


Figure 3: Same as Fig. 2, but for $N_e = 60$.

(a), which can be understood as follows. At very large M , natural inflation approximates quadratic inflation. One would therefore naively expect that for $M = 500$, the results of [38] are reproduced. Indeed, this holds from $\alpha = 0$ up to the maximum of n_s (the corresponding value for α depends on n). The “knee” is located precisely in the strong coupling limit studied in [38]:

$$r(n) \simeq \frac{8(2-n)}{N_e}, \quad (3.6)$$

$$n_s(n) \simeq 1 - \frac{3-n}{N_e}, \quad (3.7)$$

where we remind the reader that $1 < n < 2$. These predictions correspond precisely to those of monomial inflation with power $\bar{n} = 2(2-n)$ in the large- N_e approximation. Therefore, when the “knee” is reached, the model effectively behaves like $\phi^{\bar{n}}$ inflation. As α increases, the predictions remain approximately stable around this configuration, but ζ_N (and consequently ϕ_N and χ_N) slowly grows. Eventually, the shape of the potential in the inflationary region ceases to resemble a monomial form and becomes hilltop-like, explaining the subsequent turn towards lower values of n_s . To visualize all this in terms of the scalar field potential, we show in Fig. 4 the Einstein-frame potential $U(\chi)$ for $\alpha = 0$ (brown), $\alpha = 3.16 \cdot 10^6$ (black, continuous), $\alpha = 10^7$ (black, dashed), and $\alpha = 10^8$ (black, dotted), with $M = 500$ and $n = 7/4$ (left), alongside a zoomed-in view of the same potential around the minimum

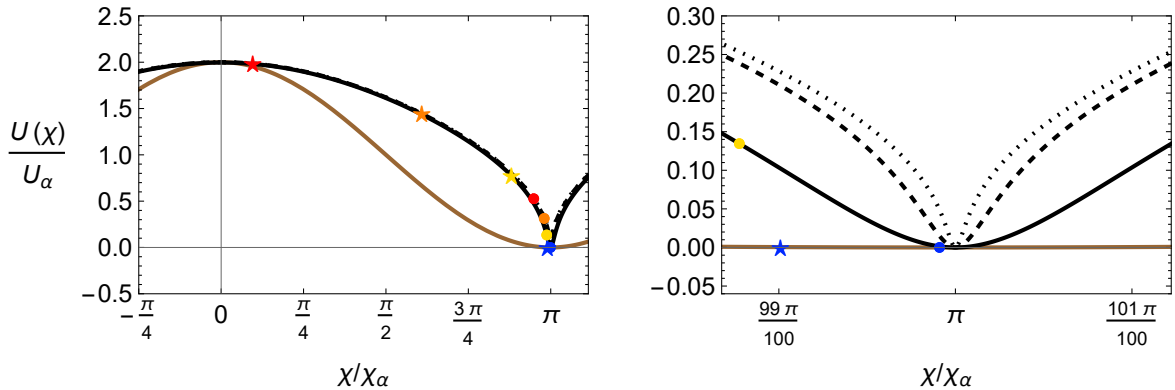


Figure 4: The Einstein-frame potential $U(\chi)$ for $\alpha = 0$ (brown), $\alpha = 3.16 \cdot 10^6$ (black, continuous), $\alpha = 10^7$ (black, dashed), and $\alpha = 10^8$ (black, dotted), with $M = 500$ and $n = 7/4$ (left), along with a zoomed-in view of the same potential (right). We indicate χ_N (stars) and χ_{end} (dots) for $\alpha = 0$ (blue), $3.16 \cdot 10^6$ (yellow), 10^7 (orange), and 10^8 (red). The value $\alpha = 3.16 \cdot 10^6$ corresponds to the maximum of n_s , i.e., the “knee” in Fig. 3. The potentials are normalized by U_α (defined in Eq. (3.8)) and the Einstein-frame canonical field χ by χ_α (defined in Eq. (3.10)), so that the potential appears with a period of 2π in the plot. Further details are given in the text.

(right). Notice that in Fig. 4 the potentials are normalized by:

$$U_\alpha \equiv 2U(\zeta_{\text{max}}), \quad (3.8)$$

with ζ_{max} defined as the value of ζ satisfying:

$$2\Lambda^4 = G(\zeta). \quad (3.9)$$

Moreover, the Einstein-frame canonical field χ is normalized by χ_α , defined as:

$$\chi_\alpha = \frac{1}{\pi} \int_0^{\zeta_{\text{max}}} \frac{1}{g(\zeta)} d\zeta, \quad (3.10)$$

so that it appears with a period of 2π in the plot. The subscript α emphasizes that U_α and χ_α depend on α . We indicate χ_N (stars) and χ_{end} (dots) for $\alpha = 0$ (blue), $3.16 \cdot 10^6$ (yellow), 10^7 (orange), and 10^8 (red). The value $\alpha = 3.16 \cdot 10^6$ corresponds to the maximum of n_s , i.e., the “knee” in Fig. 3. For sufficiently small α ² the higher-order term is negligible, and the Einstein-frame potential coincides with the Jordan-frame potential. Once the higher-order term starts dominating, up to $\alpha \lesssim 3.16 \cdot 10^6$, the Einstein-frame potential can be approximated by a monomial potential with $\bar{n} = 2(2 - n)$ in the inflationary region. For larger α , this approximation breaks down, causing n_s to decrease and producing the “tail” towards lower scalar spectral index values observed in panel (a) of Fig. 2 and 3.

²It can be computed numerically that for $n = 7/4$ and $M = 500$, the higher-order contribution becomes relevant for $\alpha \gtrsim 3 \cdot 10^5$ (see Figs. 2 and 3).

In panel (d), the predictions for Λ as a function of $\log_{10}(\alpha)$ are obtained by imposing $A_s \simeq 2.1 \cdot 10^{-9}$. The behavior of Λ directly reflects the “knee” structure seen in panel (a). It initially increases up to a maximum value:

$$\Lambda \simeq M^{\frac{1}{2}} \left[\frac{3\pi^2(2-n)A_s\alpha}{2^{2-3n} \left(\frac{n}{N_e}\right)^{n-3}} \right]^{\frac{1}{4(2-n)}}, \quad (3.11)$$

which corresponds to the $\phi^{\bar{n}}$ inflation limit, after which it decreases as α increases.

The predicted values of r tend to be relatively high, with only scenarios featuring both large α ($\gtrsim 10^6$) and large M ($M \geq 10$ for $N_e = 50$ and $M \geq 6$ for $N_e = 60$ in our ensemble) being consistent with the cosmological data. Depending on the specific parameter values, the predictions can agree with the constraints from the BICEP/Keck collaboration, the ACT collaboration, or both.

For $N_e = 50$, compatibility with the ACT combination at $\lesssim 2\sigma$ is achieved for $M > 10$ ($M = 500$ in our ensemble) and $n \gtrsim 7/4$, within an α range that depends on n , roughly 10^6 – 10^8 . Compatibility with the BICEP/Keck combination at $\lesssim 2\sigma$ is obtained already for lower values, $M \gtrsim 10$, provided $n \gtrsim 7/4$. Simultaneous compatibility with both combinations is achieved for $n \gtrsim 7/4$, $M > 10$ ($M = 500$ in our ensemble), and $\alpha \sim 10^7$ – 10^8 .

Increasing the number of e -folds to $N_e = 60$ (Fig. 3) shifts the predictions toward lower r and slightly higher n_s , allowing the $M = 6$ predictions to fall within the 95% confidence regions of the BICEP/Keck combination. Compatibility with the ACT combination at $\lesssim 2\sigma$ is achieved for $M \gtrsim 10$ and $n \gtrsim 7/4$, within an n -dependent range of α , roughly between 10^6 and 10^8 . Agreement with both combinations is realized for $n \gtrsim 7/4$, $10 < M < 500$, and $\alpha \sim 10^7$ – 10^8 .

4 Natural inflation for $n > 2$

We now consider the case with $n > 2$. The CMB observables are still given by Eqs. (3.2) and (3.5). However, a crucial difference arises: the function $G(\zeta)$ is now positive only in the range:

$$0 < \zeta < \zeta_0, \quad (4.1)$$

with $\zeta_0 \equiv (\alpha(n-2))^{\frac{1}{1-n}}$. At the same time, the function reaches its maximum at:

$$\zeta_M = (\alpha(n-2)n)^{\frac{1}{1-n}}, \quad (4.2)$$

for which:

$$G(\zeta_M) = \frac{n-1}{4n} \zeta_M. \quad (4.3)$$

As it can be understood from Fig. 1, given the shape of $G(\zeta)$ we have two possibilities for mapping ζ to ϕ . The first is to consider the range $0 < \zeta < \zeta_M$, while the other is to consider $\zeta_M < \zeta < \zeta_0$. However, in the latter range it can be shown numerically that we always have $\epsilon(\zeta) \ll 1$ which doesn’t allow a graceful exit from inflation. For this reason, in what follows we only consider the $0 < \zeta < \zeta_M$ range. Moreover, we need to require $G(\zeta_M) \geq 2\Lambda^4$ in order to ensure that the mapping between the Jordan-frame and Einstein-frame potentials is well defined. This represents the main difference with the $n < 2$ case. From Eqs. (4.2) and (4.3),

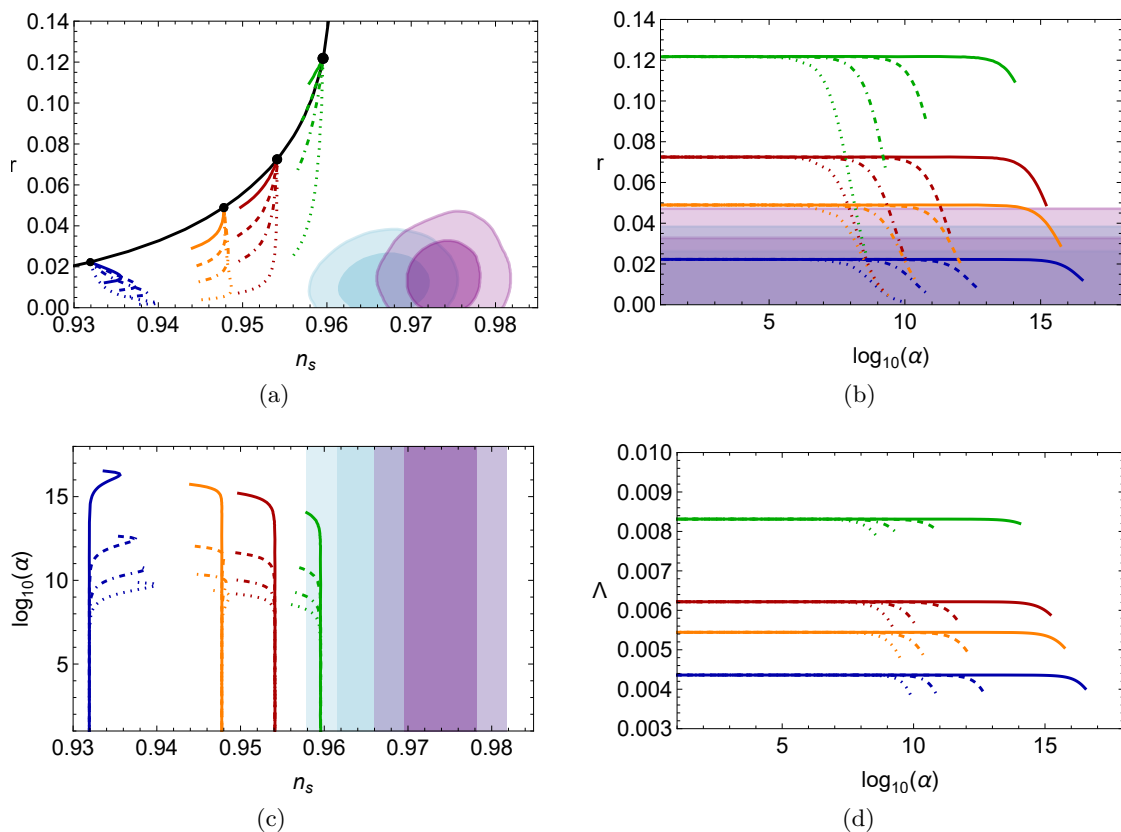


Figure 5: (a) r vs. n_s , (b) r vs. $\log_{10}(\alpha)$, (c) n_s vs. $\log_{10}(\alpha)$, and (d) Λ vs. $\log_{10}(\alpha)$ for $n > 2$ and $N_e = 50$, with $M = 4$ (blue), $M = 5$ (orange), $M = 6$ (red), and $M = 10$ (green), and $n = 3$ (continuous), $n = 5/2$ (dashed), $n = 9/4$ (dot-dashed), and $n = 33/16$ (dotted). Contours indicate the 68% and 95% confidence levels based on the latest combinations from the BICEP/Keck [9] (cyan) and ACT [47] (purple) collaborations.

we see that this condition cannot be satisfied for arbitrary values of α , as $G(\zeta_M)$ decreases with increasing α . The maximum allowed value of α can therefore be computed as:

$$\alpha_M = \frac{1}{n(n-2)} \left(\frac{n-1}{8n\Lambda^4} \right)^{n-1}. \quad (4.4)$$

Figures 5 and 6 show the results, respectively for $N_e = 50$ and $N_e = 60$, for (a) r vs. n_s , (b) r vs. $\log_{10}(\alpha)$, (c) n_s vs. $\log_{10}(\alpha)$, and (d) Λ vs. $\log_{10}(\alpha)$, with $M = 4$ (blue), $M = 5$ (orange), $M = 6$ (red), and $M = 10$ (green), and $n = 3$ (continuous), $n = 5/2$ (dashed), $n = 9/4$ (dot-dashed), and $n = 33/16$ (dotted). The amplitude of the power spectrum, A_s , is fixed to its observed value, $A_s \simeq 2.1 \cdot 10^{-9}$ [8]. Contours indicate the 68% and 95% confidence levels based on the latest combinations from the BICEP/Keck [9] (cyan) and ACT [47] (purple) collaborations.

We observe that, since α cannot increase indefinitely, the predictions for r vs. n_s remain largely ruled out as $n \rightarrow 2$. This behavior is qualitatively similar to that reported in [27] for the class of $F(R, X)$ theories, although the quantitative predictions for the CMB observables

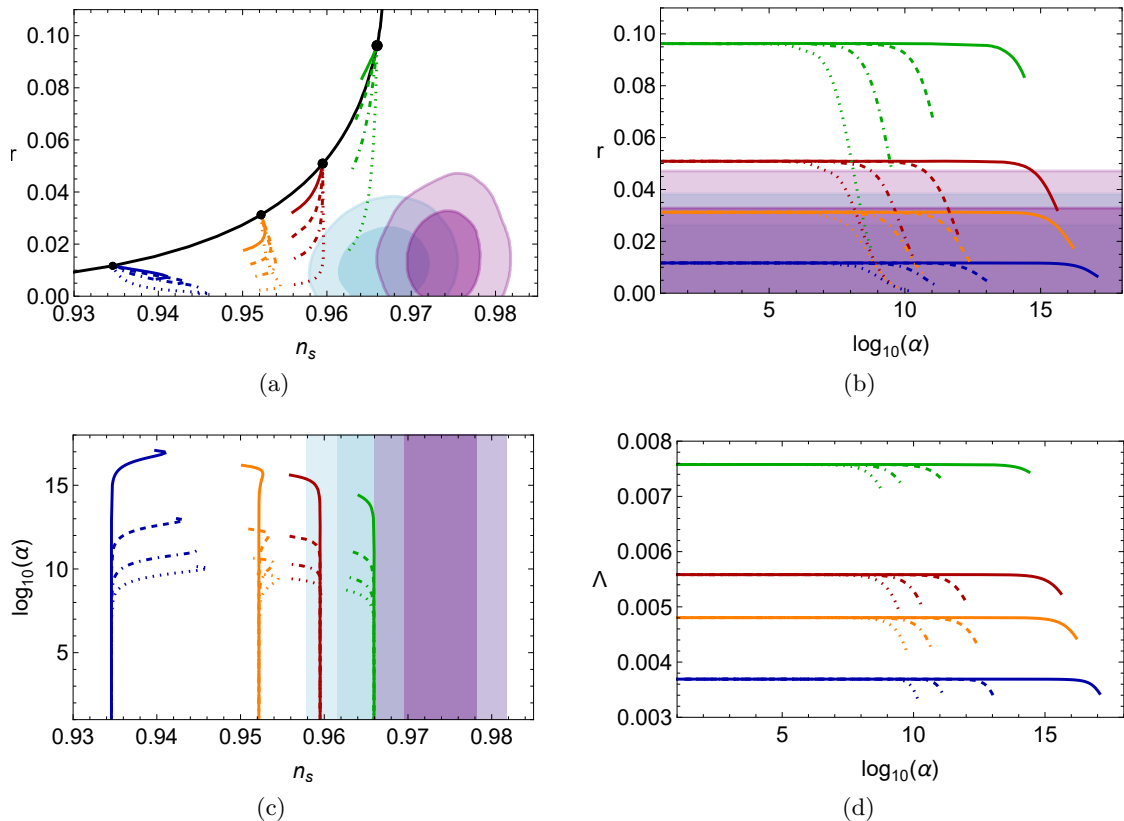


Figure 6: Same as Fig. 5, but for $N_e = 60$.

differ. Partial agreement with the BICEP/Keck combination can only be achieved for $n \rightarrow 2$, with $M \gtrsim 6$ at $N_e = 60$ and $\alpha \gtrsim 10^8$. We therefore conclude that natural inflation can be rescued when embedded in $F(R)_{>2}$ Palatini gravity, but only within a restricted region of the parameter space.

5 Conclusions

We have analyzed natural inflation within the Palatini $F(R)$ framework, considering $F(R) = R + \alpha R^n$. Our results show that for $n < 2$, the model can improve upon the predictions of standard natural inflation, particularly for $M \gtrsim 10$ and $7/4 \lesssim n \leq 2$, with α lying within an appropriate n -dependent range. In this regime, the predictions for r and n_s can satisfy the constraints from the BICEP/Keck and/or ACT combinations.

For $n > 2$, however, the allowed values of α are constrained by the observed scalar amplitude $A_s = 2.1 \cdot 10^{-9}$ and by the consistency of the equation of motion of the auxiliary field (Eq. 2.8), which limits the contribution of the higher-order term to the inflationary dynamics. Consequently, r remains relatively high and n_s does not shift sufficiently, preventing full agreement with observational constraints. Partial agreement can only be achieved for $n \rightarrow 2$, if $M \gtrsim 6$ and $\alpha \gtrsim 10^8$.

These results highlight that Palatini $F(R)$ corrections can resolve the compatibility issues of natural inflation with observations, but only within specific parameter ranges.

Acknowledgments

This work was supported by the Estonian Research Council through grants PRG1055, RVTT3, and RVTT7, as well as the CoE program TK202 “Foundations of the Universe”. This article is based on work carried out within COST Actions COSMIC WISPerS CA21106 and CosmoVerse CA21136, supported by COST (European Cooperation in Science and Technology).

References

- [1] P. Collaboration, *Planck 2018 results. vi. cosmological parameters*, *Astronomy & Astrophysics* **641** (2020) A6.
- [2] S. Alam and et al., *The clustering of galaxies in the completed sdss-iii baryon oscillation spectroscopic survey*, *Mon. Not. Roy. Astron. Soc.* **470** (2017) 2617.
- [3] M. Colless and et al., *The 2df galaxy redshift survey: spectra and redshifts*, *Mon. Not. Roy. Astron. Soc.* **328** (2001) 1039.
- [4] A. A. Starobinsky, *A New Type of Isotropic Cosmological Models Without Singularity*, *Phys. Lett.* **B91** (1980) 99.
- [5] A. H. Guth, *The Inflationary Universe: A Possible Solution to the Horizon and Flatness Problems*, *Phys.Rev.* **D23** (1981) 347.
- [6] A. D. Linde, *A New Inflationary Universe Scenario: A Possible Solution of the Horizon, Flatness, Homogeneity, Isotropy and Primordial Monopole Problems*, *Phys.Lett.* **B108** (1982) 389.
- [7] A. Albrecht and P. J. Steinhardt, *Cosmology for Grand Unified Theories with Radiatively Induced Symmetry Breaking*, *Phys.Rev.Lett.* **48** (1982) 1220.
- [8] PLANCK collaboration, *Planck 2018 results. X. Constraints on inflation*, *Astron. Astrophys.* **641** (2020) A10 [[1807.06211](#)].
- [9] BICEP, KECK collaboration, *Improved Constraints on Primordial Gravitational Waves using Planck, WMAP, and BICEP/Keck Observations through the 2018 Observing Season*, *Phys. Rev. Lett.* **127** (2021) 151301 [[2110.00483](#)].
- [10] K. Freese, J. A. Frieman and A. V. Olinto, *Natural inflation with pseudo - Nambu-Goldstone bosons*, *Phys. Rev. Lett.* **65** (1990) 3233.
- [11] J. E. Kim, H. P. Nilles and M. Peloso, *Completing natural inflation*, *JCAP* **01** (2005) 005 [[hep-ph/0409138](#)].
- [12] L. Visinelli, *Natural Warm Inflation*, *JCAP* **09** (2011) 013 [[1107.3523](#)].
- [13] A. Achúcarro, V. Atal and Y. Welling, *On the viability of $m^2\phi^2$ and natural inflation*, *JCAP* **07** (2015) 008 [[1503.07486](#)].
- [14] R. Z. Ferreira, A. Notari and G. Simeon, *Natural Inflation with a periodic non-minimal coupling*, *JCAP* **11** (2018) 021 [[1806.05511](#)].
- [15] I. Antoniadis, A. Karam, A. Lykkas, T. Pappas and K. Tamvakis, *Rescuing Quartic and Natural Inflation in the Palatini Formalism*, *JCAP* **1903** (2019) 005 [[1812.00847](#)].
- [16] A. Salvio, *Quasi-Conformal Models and the Early Universe*, *Eur. Phys. J. C* **79** (2019) 750 [[1907.00983](#)].

- [17] G. Simeon, *Scalar-tensor extension of Natural Inflation*, *JCAP* **07** (2020) 028 [2002.07625].
- [18] E. McDonough, A. H. Guth and D. I. Kaiser, *Nonminimal Couplings and the Forgotten Field of Axion Inflation*, 2010.04179.
- [19] A. Salvio, *Natural-scalaron inflation*, *JCAP* **10** (2021) 011 [2107.03389].
- [20] A. Salvio, *BICEP/Keck data and quadratic gravity*, *JCAP* **09** (2022) 027 [2202.00684].
- [21] N. Bostan, *Non-minimally coupled Natural Inflation: Palatini and Metric formalism with the recent BICEP/Keck*, *JCAP* **02** (2023) 063 [2209.02434].
- [22] A. Salvio and S. Sciusco, *(Multi-field) natural inflation and gravitational waves*, *JCAP* **03** (2024) 018 [2311.00741].
- [23] A. Mukuno and J. Soda, *Chromonatural warm inflation*, *Phys. Rev. D* **109** (2024) 123504 [2402.08849].
- [24] A. Racioppi and A. Salvio, *Natural metric-affine inflation*, *JCAP* **06** (2024) 033 [2403.18004].
- [25] D. L. Lorenzoni, D. I. Kaiser and E. McDonough, *Natural inflation with exponentially small tensor-to-scalar ratio*, *Phys. Rev. D* **110** (2024) L061302 [2405.13881].
- [26] M. Michelotti, R. Gonzalez Quaglia, E. Dimastrogiovanni, M. Fasiello and D. Roest, *Kinetic Gauge Friction in Natural Inflation*, 2411.19892.
- [27] N. Bostan, R. H. Dejarah, C. Dioguardi and A. Racioppi, *Natural inflation in Palatini $F(R, X)$* , *JCAP* **07** (2025) 082 [2503.16324].
- [28] T. Koivisto and H. Kurki-Suonio, *Cosmological perturbations in the palatini formulation of modified gravity*, *Class. Quant. Grav.* **23** (2006) 2355 [astro-ph/0509422].
- [29] F. Bauer and D. A. Demir, *Inflation with Non-Minimal Coupling: Metric versus Palatini Formulations*, *Phys. Lett.* **B665** (2008) 222 [0803.2664].
- [30] L. Järv, A. Karam, A. Kozak, A. Lykkas, A. Racioppi and M. Saal, *Equivalence of inflationary models between the metric and Palatini formulation of scalar-tensor theories*, *Phys. Rev. D* **102** (2020) 044029 [2005.14571].
- [31] I. D. Gialamas, A. Karam, T. D. Pappas and E. Tomberg, *Implications of Palatini gravity for inflation and beyond*, *Int. J. Geom. Meth. Mod. Phys.* **20** (2023) 2330007 [2303.14148].
- [32] V.-M. Enckell, K. Enqvist, S. Rasanen and L.-P. Wahlman, *Inflation with R^2 term in the Palatini formalism*, *JCAP* **1902** (2019) 022 [1810.05536].
- [33] I. Antoniadis, A. Karam, A. Lykkas and K. Tamvakis, *Palatini inflation in models with an R^2 term*, *JCAP* **1811** (2018) 028 [1810.10418].
- [34] I. D. Gialamas and A. B. Lahanas, *Reheating in R^2 Palatini inflationary models*, 1911.11513.
- [35] I. D. Gialamas, A. Karam and A. Racioppi, *Dynamically induced Planck scale and inflation in the Palatini formulation*, *JCAP* **11** (2020) 014 [2006.09124].
- [36] K. Dimopoulos and S. Sánchez López, *Quintessential inflation in Palatini $f(R)$ gravity*, *Phys. Rev. D* **103** (2021) 043533 [2012.06831].
- [37] A. Karam, E. Tomberg and H. Veermäe, *Tachyonic preheating in Palatini R^2 inflation*, *JCAP* **06** (2021) 023 [2102.02712].
- [38] C. Dioguardi, A. Racioppi and E. Tomberg, *Slow-roll inflation in Palatini $F(R)$ gravity*, *JHEP* **06** (2022) 106 [2112.12149].
- [39] K. Dimopoulos, A. Karam, S. Sánchez López and E. Tomberg, *Modelling Quintessential Inflation in Palatini-Modified Gravity*, *Galaxies* **10** (2022) 57 [2203.05424].
- [40] K. Dimopoulos, A. Karam, S. Sánchez López and E. Tomberg, *Palatini R^2 quintessential inflation*, *JCAP* **10** (2022) 076 [2206.14117].

- [41] C. Dioguardi, A. Racioppi and E. Tomberg, *Beyond (and back to) Palatini quadratic gravity and inflation*, *JCAP* **03** (2024) 041 [[2212.11869](#)].
- [42] C. Dioguardi and A. Racioppi, *Palatini $F(R, X)$: a new framework for inflationary attractors*, [2307.02963](#).
- [43] H. J. Kuralkar, S. Panda and A. Vidyarthi, *Observable primordial gravitational waves from non-minimally coupled R^2 Palatini modified gravity*, *JCAP* **05** (2025) 073 [[2502.03573](#)].
- [44] C. Dioguardi and A. Karam, *Palatini linear attractors are back in action*, *Phys. Rev. D* **111** (2025) 123521 [[2504.12937](#)].
- [45] C. Dioguardi, A. J. Iovino and A. Racioppi, *Fractional attractors in light of the latest ACT observations*, *Phys. Lett. B* **868** (2025) 139664 [[2504.02809](#)].
- [46] K. Dimopoulos, C. Dioguardi, G. Hütsi and A. Racioppi, *Quintessential Inflation in Palatini $F(R, X)$ gravity*, [2503.21610](#).
- [47] ACT collaboration, *The Atacama Cosmology Telescope: DR6 Constraints on Extended Cosmological Models*, [2503.14454](#).